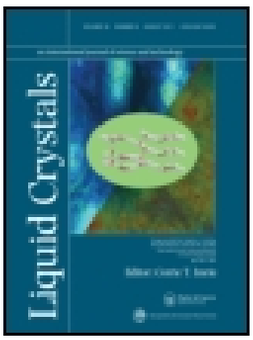

Liquid Crystals

ISSN: (Print) (Online) Journal homepage: https://www.tandfonline.com/loi/tlct20

Quantitative error analysis for non-mechanical phase-controlled beam steering based on symmetrical radial sub-aperture coherence algorithm

Cheng-Miao Wang , Wan Chen , Zhi-Wei Zhao , Quan-Quan Mu , Zheng-Hui Peng , Zhi-Hui Diao , Li-Shuang Yao , Li Xuan & Qi-Dong Wang

To cite this article: Cheng-Miao Wang , Wan Chen , Zhi-Wei Zhao , Quan-Quan Mu , Zheng-Hui Peng , Zhi-Hui Diao , Li-Shuang Yao , Li Xuan & Qi-Dong Wang (2020): Quantitative error analysis for non-mechanical phase-controlled beam steering based on symmetrical radial sub-aperture coherence algorithm, Liquid Crystals, DOI: 10.1080/02678292.2020.1783706

To link to this article: https://doi.org/10.1080/02678292.2020.1783706

Published online: 02 Aug 2020.

Submit your article to this journal

Article views: 23

View related articles

View Crossmark data

Full Terms & Conditions of access and use can be found at
https://www.tandfonline.com/action/journalInformation?journalCode=tlct20

LIQUID CRYSTALS
https://doi.org/10.1080/02678292.2020.1783706

Taylor & Francis
Taylor & Francis Group

Check for updates

Quantitative error analysis for non-mechanical phase-controlled beam steering based on symmetrical radial sub-aperture coherence algorithm

Cheng-Miao Wang[a,b], Wan Chen[a,b], Zhi-Wei Zhao[a,b], Quan-Quan Mu[a,b], Zheng-Hui Peng[a], Zhi-Hui Diao[a], Li-Shuang Yao[c], Li Xuan[a,b] and Qi-Dong Wang[a]

[a]State Key Laboratory of Applied Optics, Changchun Institute of Optics, Fine Mechanics and Physics, Chinese Academy of Sciences, Changchun, Jilin, China; [b]Center of Materials Science and Optoelectronics Engineering, University of Chinese Academy of Sciences, Beijing, China; [c]Department of Physics, College of Science, Shantou University, Shantou, China

ABSTRACT

Based on the fundamental of traditional Sub-aperture coherence (SAC) algorithm, Radial Sub-aperture coherence (RSAC) and Symmetrical Radial Sub-aperture coherence (SRSAC) have been designed to achieve non-mechanical beam steering with ultra-high precision and stability by utilising two-dimensional Liquid Crystal Optical Phased Array (LCOPA). Both of them inherit the original advantages, that is, to eliminate the local pointing accuracy defects and greatly improve the angular resolution of the beam steering system. Meanwhile, the steering angle error caused by the aperture variation and the alignment error can be also effectively restricted by SRSAC. In this paper, the essential mathematical framework of SRSAC and its affiliated local error elimination method was established to supplement the theoretical support of these phase generation algorithms. By dissecting the generation mechanism of each pointing error branch, the theoretical formulae with great universality are finally proposed, which provide visualised and necessary references for the specific application in other beam control situations.

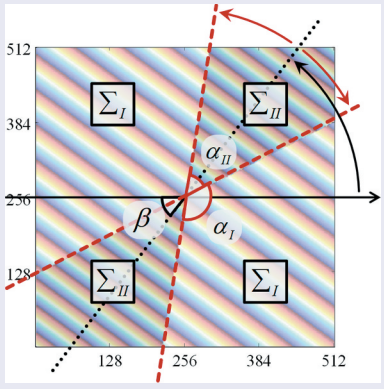

ARTICLE HISTORY
Received 3 January 2020
Accepted 14 June 2020

KEYWORDS
Liquid crystal optical phased array; beam steering; sub-aperture coherence; symmetrical radial sub-aperture coherence; pointing accuracy

1. Introduction

As a typical non-mechanical beam steering technique, LCOPA [1–5] has broad application prospects in lidar [6,7] and free-space optical communication [8–11] because of the advantages of agile scan, low Size Weight and Power (SWaP) consumption [12]. The parameters such as pointing accuracy, angular resolution, dynamic response speed and mechanical vibration tolerance often determine the application performance [13,14] of this type of active photoelectric system. The traditional phase generation algorithm, variable period grating (VPG) [15], is faced with the problems of local pointing accuracy defect and insufficient angular resolution. SAC algorithm, which was published on *Opt. Commun.* [16] in 2015, has solved these problems to some extent but the accuracy was strictly limited by the beam aperture deviation and the alignment error. In 2019, two new algorithms called radial sub-aperture coherence (RSAC) and symmetrical radial sub-aperture coherence (SRSAC) were proposed to solve the original problems, which could deflect the beam of the arbitrary aperture with ultra-high precision and effectively improve the stability of the scanning angle sequences in the presence of

CONTACT Li Xuan xuanli@ciomp.ac.cn; Qi-dong Wang qdwang@ciomp.ac.cn
© 2020 Informa UK Limited, trading as Taylor & Francis Group

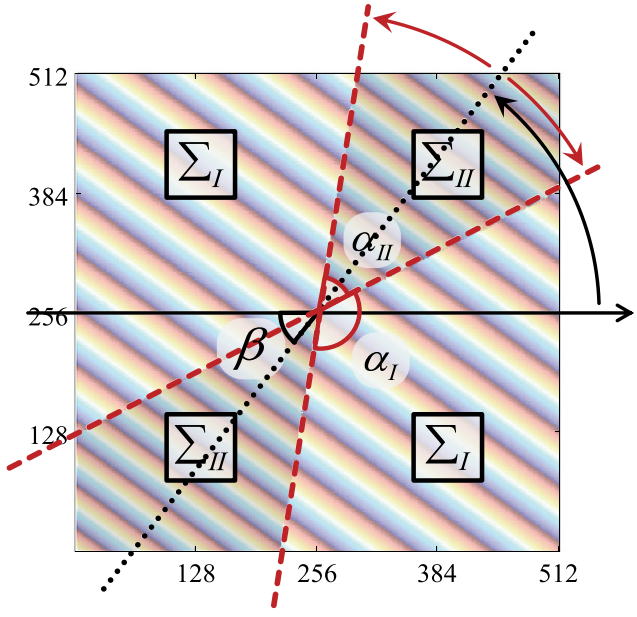

Figure 1. (Colour online) Phase diagram of SRSAC algorithm.

alignment errors [17]. On this basis, an optimisation method of SRSAC algorithm, local precision defect elimination method, was proposed to drastically cut off the pointing error residual regions in the effective steering range [18]. Thus, SRSAC can greatly improve the pointing accuracy and angular resolution under the condition of varying aperture and alignment error, which makes the ultra-high precision beam steering technology based on LCOPA have more remarkable universality and practicability in specific applications.

The core principle of SRSAC algorithm is based on VPG with lower pointing accuracy [19,20]. The modulator panel is divided into two sub-domains, respectively, loading two saw-tooth phases with slight differences, as shown in Figure 1. The symmetric double sector sub-domains enable the method to effectively deal with the complex situation of beam aperture variation and alignment error.

For a desired two-dimensional steering angle $\boldsymbol{\theta} = (\theta_x, \theta_y)$, the magnitudes of corresponding tilt angles of the two sub-domains are, respectively, shown in Equation (1).

$$\left|\vec{\theta}_I\right| = \theta_{step} \cdot floor(\left|\vec{\theta}\right|/\theta_{step}) \ , \ \left|\vec{\theta}_{II}\right| = \left|\vec{\theta}_I\right| + \theta_{step} \quad (1)$$

where θ_{step} is a constant representing the interpolation segment length. β represents the azimuth of the symmetry axis of two fan-shaped sub-domains, which is also the azimuth of steering angle θ. Meanwhile, the fine tuning of sub-domain sector angles α_I and α_{II} can be realised by referring to the pre-existing nonlinear relationship between the area occupation rate α_{II}/π and the normalised steering angle θ_{norm} [17]. The normalised steering angle is defined as shown in Equation (2).

$$\theta_{norm} = \frac{\left|\vec{\theta}\right| - \left|\vec{\theta}_I\right|}{\left|\vec{\theta}_{II}\right| - \left|\vec{\theta}_I\right|} \quad (2)$$

In this way, the equidistant and high-density steering angle output can be achieved in the whole dynamic range and the angular resolution can be greatly improved. However, the analysis of the pointing accuracy improvement based on the above conception was mainly at the qualitative level. In this paper, all kinds of error components caused by hardware imperfections are analysed and simulated seriatim. Furthermore, the performance of SRSAC in improving pointing accuracy can be summarised explicitly and quantitatively.

2. Theoretical analysis and simulation verification

2.1. Pointing accuracy of VPG

Since the phase distribution in each sub-domain of SRSAC is still loaded according to VPG, it is necessary to quantify the accuracy of this basic algorithm. From [18], the limited number of pixels in the modulator and the quantised output phase grey scale will lead to a serious decrease of pointing accuracy at some local steering ranges. According to this theory, the maximum steering error can be simply expressed as Equation 3.

$$\max(|\theta_{error}|) = \frac{\lambda}{2N_G \cdot R} \quad (3)$$

where N_G represents the preset phase greyscale number in the modulator, λ and R respectively represent the wavelength and half-diameter of the incident plane wave. These maximum error points are defined as main error peaks and appear around some special steering angles which are integer multiple of a characteristic angle $\theta_p = \lambda/N_G\ d$, where d is pixel pitch of the modulator [18].

While paying attention to the maximum error of VPG, its overall error variance also has reference significance, which is extremely difficult to estimate accurately by rigorous theoretical calculation. In [21], the RMS of pointing error is approximated as the ratio of a fixed steering angle range to the number of steering angles that can be achieved within it. On the premise that the phase origin is located in the centre of the panel, the corresponding formula can be rewritten into the form of Equation (4).

$$\sigma_{VPG} \approx 8\frac{\lambda}{N_G}\cdot\frac{d}{R^2} \tag{4}$$

Equation (4) represents 'average scanning angle interval', which is a sententious and pellucid concept of scanning accuracy and can also be used for the approximation of absolute pointing accuracy. However, in order to pursue the ultra-high accuracy of the pointing error prediction, Equation (4) needs to be further modified into a somewhat complex form. After the directly proportional relationship between σ_{VPG} and optical delay step λ/N_G was verified in simulation, the main correction targets are determined as two parameters of the additional constant of pixel pitch d and the exponent of spot size R, which can be expressed as Equation (5).

$$\sigma_{VPG} = a\cdot\frac{\lambda}{N_G}\cdot(d+d_0)\cdot R^{\delta} \tag{5}$$

Multi-parameter fitting results show that d_0 = 19.5 μm, $\delta = -1.6$ and additional coefficient a = 0.11 $\mu m^{-0.4}$. The fitting effect is shown in Figure 2, which proves the rationality of the form of the target regression function.

2.2. Weight allocation error and endpoint introduced error of SRSAC

The phase generation scheme of SRSAC is to load the VPG phase with different tilt angles in multiple regions, which mathematically corresponds to the processes of interpolation endpoint construction and weight allocation. According to Equation (6), the overall error can be seen as consisting of weight allocation error and endpoint introduced error, which is caused by the deviation of θ_{norm} and$\theta_{I,\ II}$, respectively.

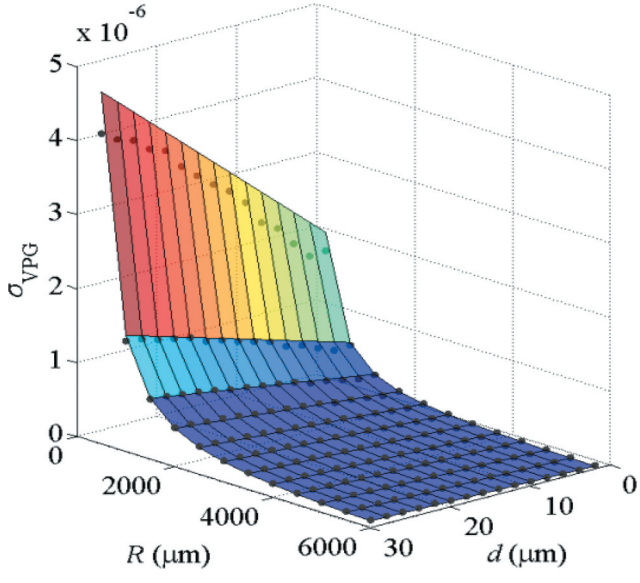

Figure 2. (Colour online) Comparison diagram of regression analysis surface and simulated scatter points of σ_{VPG}.

$$\begin{aligned}\left|\vec{\theta}\right| &= \left|\vec{\theta}_I\right| + \theta_{norm}\cdot\theta_{step}\\ &= (1-\theta_{norm})\cdot\left|\vec{\theta}_I\right| + \theta_{norm}\cdot\left|\vec{\theta}_{II}\right|\end{aligned} \tag{6}$$

Obviously, the weight allocation error σ_w and endpoint introduced error σ_e can be discussed completely separately since there is no correlation between them.

Firstly, on the premise that the position deviation of two endpoints is ignored, the form of weight allocation error can be directly obtained from Equation (6), as shown in Equation (7).

$$\sigma_w = \theta_{step}\cdot\sigma_{\theta_{norm}} \tag{7}$$

In the framework of SRSAC, the relationship betweenθ_{norm} and area occupation rate $\eta_{I,II} = \alpha_{I,II}/\pi$ is constant in arbitrary interpolating segments. However, for different steering angle regions, the scanning sequences after linearisation correction may slightly deviate from their theoretical correspondence. Since the corresponding relation between θ_{norm} and $\eta_{I,II}$ is insensitive to hardware parameters, the standard deviation of θ_{norm} is approximately constant, that is, the weight allocation error has a linear relationship with $\theta_{step.}$ After a large number of random scanning segments were selected for simulation test as shown in Figure 3, the value of $\sigma_{\theta norm}$ was verified to be 1.2%.

On the other hand, the calculation of endpoint error needs to be carried out without considering weight allocation error. In Equation (6), it is clear that the pointing error variances of endpoints θ_I and θ_{II} can be expressed in terms of $\sigma_{VPG}{}^2$; thus, $\sigma_e{}^2$ can be written as Equation (8).

$$\begin{aligned}\sigma_e^2(\theta_{norm}) &= (1-\theta_{norm})^2\sigma_{VPG}^2 + \theta_{norm}{}^2\sigma_{VPG}^2\\ &\quad + 2c\cdot(1-\theta_{norm})\theta_{norm}\sigma_{VPG}^2\\ &= [1-(2\theta_{norm}-2\theta_{norm}{}^2)(1-c)]\cdot\sigma_{VPG}^2\end{aligned} \tag{8}$$

where c is the correlation coefficient of two endpoints, which can be simplified to the expectation of the scalar product of the angular deviation vectors, as shown in Equation (9).

$$c = E\left(\vec{\theta}_I\cdot\vec{\theta}_{II}\right) - E\left(\vec{\theta}_I\right)\cdot E\left(\vec{\theta}_{II}\right) = E\left(\Delta\vec{\theta}_I\cdot\vec{\theta}_I\right)\% \tag{9}$$

As a function of the interpolation segment length, endpoint correlation coefficient can firstly provide a significant reference for the selection of θ_{step} [18] and secondly play an auxiliary role in the estimation of endpoint introduced error. On the 2D scanning plane, the expectations of error variance at each steering points

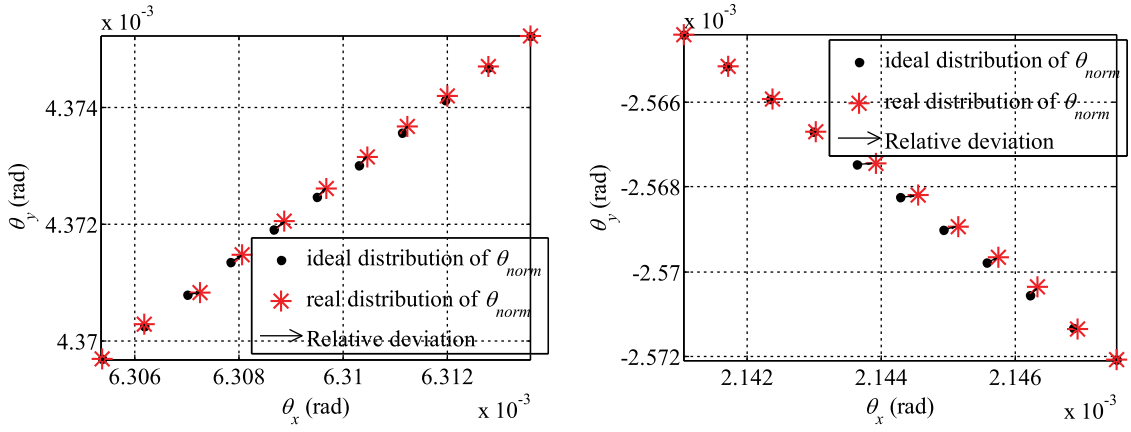

Figure 3. (Colour online) Schematic diagram of random scanning segments used to test the standard deviation of θ_{norm}.

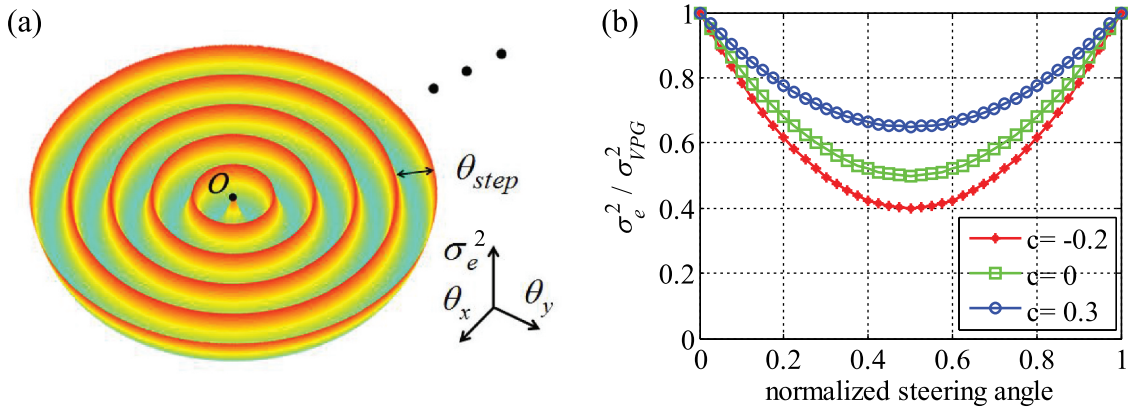

Figure 4. (Colour online) Schematic diagram of the endpoint introduced error. (a) 2D global distribution. (b) 1D distribution in an interpolation segment.

have been worked out according to Equation (8), as shown in Figure 4(a). The overall endpoint introduced error is the average value within the whole scanning range, which is also proved to be the average value within an arbitrary 1D interpolation segment length, as shown in Figure 4(b).

Therefore, the magnitude of the overall endpoint introduced error is shown in Equation (10).

$$\sigma_e^2 = \frac{1}{\pi\theta_{\max}^2}\int_0^{2\pi}\int_0^{\theta_{\max}} \sigma_e^2\left[\mathrm{mod}\left(\theta,\theta_{step}\right)/\theta_{step}\right]\theta d\theta d\varphi$$
$$= \int_0^1 \left[1-(2\theta_{norm}-2\theta_{norm}^2)(1-c)\right]\sigma_{VPG}^2 d\theta_{norm} = \frac{1}{3}(c+2)\sigma_{VPG}^2 \tag{10}$$

The symmetry of the error proportion parabola in Figure 4(b) makes the two-dimensional integral in Equation (10) greatly simplified, which also means that the conclusion in Equation (10) is compatible with both 1D and 2D applications. Furthermore, Equation (10) indicates that the endpoint introduced error of SRSAC is always smaller than that of VPG, whose physical essence is the neutralisation effect of the endpoint deviation vectors during the interpolated point generation process. Finally, the overall pointing accuracy of SRSAC can surpass that of VPG because the error suppression effect of the interpolation process is more dominant than the precision deterioration caused by the weight allocation misalignment.

Combined with the above two error sources, the overall pointing error of SRSAC can be expressed by Equation (3)

$$\sigma_{SRSAC}^2 = \sigma_w^2 + \sigma_e^2 = \left(1.2\%\cdot\theta_{step}\right)^2 + \frac{1}{3}(c+2)\sigma_{VPG}^2 \tag{11}$$

In the best case where the weight allocation error is ignored, the error variance of SRSAC may be reduced to 0.6 times of the classical VPG algorithm if the interpolation segment length is chosen appropriately to make the endpoint correlation coefficient reach −0.2. In fact, due to the inevitability of the associated weight allocation error with SRSAC, the error variance of SRSAC is almost

impossible to be suppressed as significantly as that in the ideal case or even worse than that of VPG under some extreme parametric conditions. In that sense, it is necessary to further reduce the proportional coefficient between the endpoint introduced error and $\sigma_{VPG}{}^2$ to improve the overall level of SRSAC pointing accuracy.

2.3. The precision improvement due to precision defect elimination

The interpolation segment length is always set as a constant in the standard SRSAC algorithm and the endpoint steering angles in the interpolation process are distributed equidistantly along the radial direction, regardless of whether the pointing accuracy of their positions is affected by error peaks. Since the position and width of the error peaks generated by VPG have been clarified, targeted adjustments to the positions of interpolation endpoints falling into error peaks can be meticulously made [18]. This endpoint adjustment process is unquestionable for the removal of error peaks, as shown in Figure 5, but the magnitude of the overall accuracy improvement needs to be analysed in depth.

The essence of the local precision defect elimination method to suppress the global error is to refine the set of alternative interpolation endpoints. New available interpolation endpoints will have a significant reduced pointing error variance after the local defect points are eliminated, even if the number of removal points is only $d/R\chi 100\%$ of the total. The sets of endpoints before and after error peak elimination are shown in Figure 6, in which the highest order of the eliminated error peak defaults to 4.

If the ratio of error standard deviation before and after error peak elimination is used to describe the performance improvement of global accuracy, this ratio will obviously not be affected by the proportional scaling of the initial error peak distribution structure in Figure 6(a), which is determined by the step height of the light delay λ/N_G. Furthermore, the pixel pitch d determines the distribution density of error peaks and the beam half-aperture R determines the height and width of error peaks. Under the default condition that $d \ll R$, both of them have no obvious influence on the pointing accuracy improvement caused by the endpoint set refinement, as shown in Figure 7.

Therefore, the contribution of error peak elimination to the pointing accuracy improvement can be regarded as multiplying the original error standard deviation by a constant factor less than 1. Taking the most commonly used error peak elimination method as an example, in which the highest order of removed error peaks is order 4, the ratio of RMS of the pointing error before and after removing error peaks is about 0.48, with a deviation of less than 5%. Finally, Equation (11) can be further optimised, as shown in Equation (12).

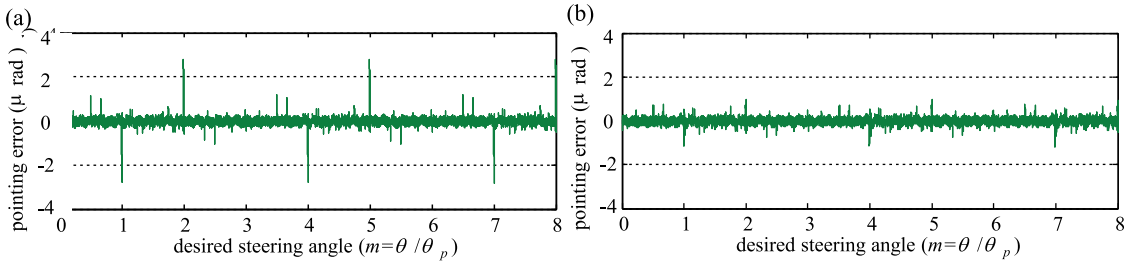

Figure 5. (Colour online) Comparison diagram of overall 1D accuracy before and after error peak elimination. (a) Before elimination. (b) After elimination.

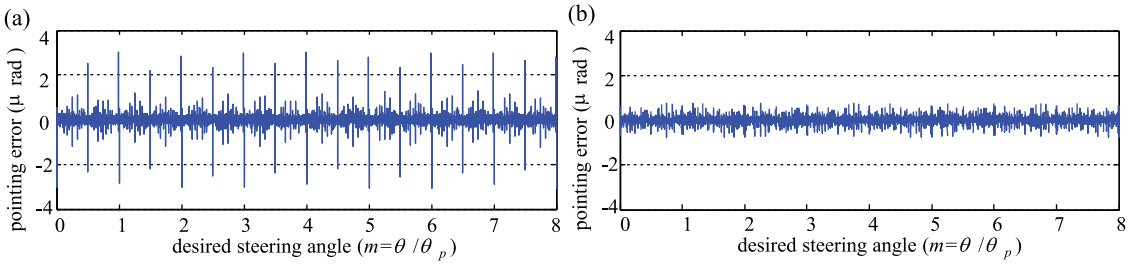

Figure 6. (Colour online) Error distribution of alternative interpolation endpoints before and after error peak elimination. (a) Before elimination. (b) After elimination.

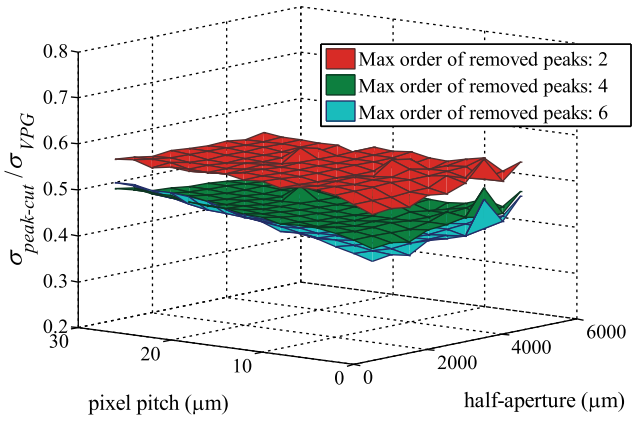

Figure 7. (Colour online) Simulation schematic diagram of pointing error suppression performance under different external parameters.

$$\sigma_{SRSAC}^2 = \sigma_w^2 + \sigma_e^2 = \left(1.2\% \cdot \theta_{step}\right)^2 + \frac{1}{3}(c+2)\left(0.48 \cdot \sigma_{VPG}\right)^2 \quad (12)$$

For Equation (12), the weight allocation error represented by the former term is already the conclusion of induction type, so the simulation verification of Equation (12) is mainly to verify the accuracy of its latter item, that is, the endpoint introduced error, which is a rule predicted by deductive logic. According to Equation (5), the system structure parameters were set carefully to compare the RMS of pointing error generated by VPG and the SRSAC algorithm with precision defect elimination method, as shown in Figure 8.

In Figure 8, the correlation coefficient between endpoints defaults to 0 and the interpolated segment length defaults to 10μrad. If the intersection point of the straight line with the same error RMS and the error relation curve is defined as cut-off point, the error region that needs to be verified is the region after the cut-off point, that is, the valid region. It can be intuitively seen that the simulated sampling points fluctuate up and down slightly around the theoretical prediction curve in the valid region, which proves the reliability of Equation (12). On this basis, it can be inferred that SRSAC algorithm has a particularly obvious improvement for those modulators whose hardware parameters are not very excellent and the pointing accuracy of traditional VPG algorithm is unsatisfactory.

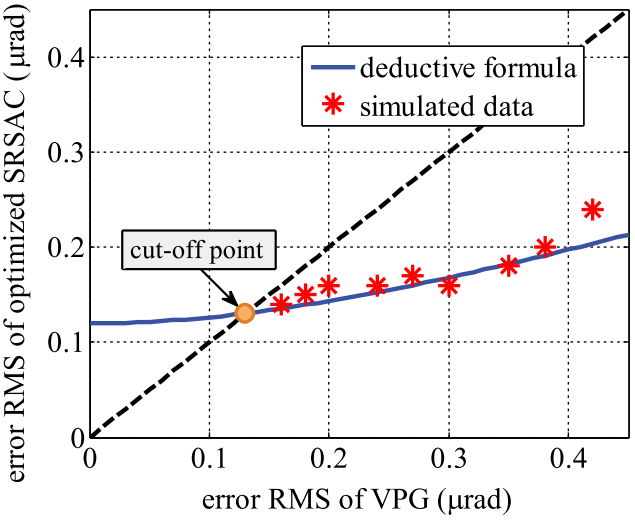

Figure 8. (Colour online) Schematic diagram of the pointing error RMS relationship between VPG and optimised SRSAC.

3. Conclusion

In the non-mechanical beam steering control technology, a new phase generation algorithm called SRSAC based on the liquid crystal spatial light modulator has been established, which effectively improve the global pointing accuracy of the scanning system. In this paper, we first propose the theoretical framework of the algorithm, two kinds of error sources that constitute the SRSAC pointing error, namely weight allocation error and endpoint introduced error, were analysed by induction and deduction, respectively. On this basis, the global error suppression effect of the precision defect elimination method was reasonably simplified and a relatively sophisticated mathematical model for predicting the performance of SRSAC pointing accuracy was obtained. Finally, the reliability of the error prediction formula was verified again through the simulation experiment, which provided a convenient and persuasive theoretical analysis approach for the extensive application of SRSAC.

Acknowledgments

This work was supported by the National Natural Science Foundation of China and State Key Laboratory of Applied Optics, Changchun Institute of Optics, Fine Mechanics and Physics, Chinese Academy of Sciences.

Disclosure statement

No potential conflict of interest was reported by the author(s).

Funding

This work was sponsored by the National Natural Science Foundation of China [11604327, 11974345, 11704378, 61975202 and 61775212].

References

[1] Mcmanamon PF, Dorschner TA, Corkum DL, et al. Optical phased array technology. Proc IEEE. 1996;84 (2):268–298.

[2] Zhang Z, You Z, Chu D. Fundamentals of phase-only liquid crystal on silicon (LCOS) devices. Light Sci Appl. 2014;3(10):213.

[3] Vettese D. Microdisplays: liquid crystal on silicon. Nat Photonics. 2011;4(11):752–754.

[4] Choubey A, Andros F, Sammakia B. Study of assembly processes for liquid crystal on silicon (LCoS) microdisplays. Proceedings of the Ninth Intersociety Conference on Thermal and Thermomechanical Phenomena in Electronic Systems; 2004 Jun 1–4; Las Vegas, NV.

[5] Zhang Z, Jeziorska-Chapman AM, Collings N, et al. High quality assembly of phase-only liquid crystal on silicon (LCOS) devices. J Disp Technol. 2011;7 (3):120–126.

[6] Seldomridge NL, Shaw JA, Repasky KS. Dual-polarization lidar using a liquid crystal variable retarder. Opt Eng. 2006;45(10):106202.

[7] Wang Y, Wu MC. An optical phased array for LIDAR. J Phys Conf Ser. 2016;772(1):012004.

[8] Lin Y, Mahajan M, Taber D, et al. Compact 4 cm aperture transmissive liquid crystal optical phased array for free-space optical communications. Proceedings of SPIE 5892, Optics and Photonics 2005; 2005 Aug 31; San Diego, CA.

[9] Miniscalco WJ, Lane SA. Optical space-time division multiple access. J Lightwave Technol. 2012;30 (11):1771–1785.

[10] Winker B, Mahajan M, Hunwardsen M. Liquid crystal beam directors for airborne free-space optical communications. Proceedings of IEEE, Aerospace Conference; 2004 Mar 6–14; Big Sky, MT.

[11] Guo Q, Xu L, Sun JT, et al. Fast switching beam steering based on ferroelectric liquid crystal phase shutter and polarisation grating. Liq Cryst. 2019;46:1383–1388.

[12] Wang X, Wu L, He X, et al. Theoretical analysis on power stability and switch time of the non-mechanical beam steering using liquid crystal optical phased array. Liq Cryst. 2018;45(10):1477–1486.

[13] Wang X, Xu J, Huang Z, et al. Theoretical model and experimental verification on the PID tracking method using liquid crystal optical phased array. Proceedings of SPIE 10096, SPIE LASE; 2017 Feb 24; San Francisco, CA.

[14] Haellstig E, Stigwall J, Lindgren M, et al. Laser beam steering and tracking using a liquid crystal spatial light modulator. Proceedings of SPIE 5087, AeroSense 2003; 2003 Aug 21; Orlando, FL.

[15] Mcmanamon PF, Bos PJ, Escuti MJ, et al. A review of phased array steering for narrow-band electrooptical systems. Proc IEEE. 2009;97(6):1078–1096.

[16] Tang Z, Wang X, Huang Z, et al. Sub-aperture coherence method to realize ultra-high resolution laser beam deflection. Opt Commun. 2015;335:1–6.

[17] Wang C, Peng Z, Liu Y, et al. Radial sub-aperture coherence method used to achieve beam steering with high precision and stability. Opt Express. 2019;27 (5):6331–6347.

[18] Wang C, Peng Z, Liu Y, et al. Two-dimensional symmetrical radial sub-aperture coherence and the local precision defect elimination method for high-precision beam steering. Opt Express. 2019;27 (13):18751–18765.

[19] Engström D, Bengtsson J, Eriksson E, et al. Steering accuracy of a spatial light modulator-based single beam steerer: guidelines and limitations. Proceedings of SPIE 7038, NanoScience + Engineering; 2008 Aug 29; San Diego, CA.

[20] Linnenberger A, Serati S, Stockley J. Advances in optical phased array technology. Proceedings of SPIE 6304, SPIE Optics + Photonics; 2006 Sep 1; San Diego, CA.

[21] Engström D, Bengtsson JR, Eriksson E, et al. Improved beam steering accuracy of a single beam with a 1D phase-only spatial light modulator. Opt Express. 2008;16(22):18275–18287.